GROUP VAPORIZATION OF LIQUID FUEL SPRAYS

Suk Ho Lee*

(*Received October 25, 1989*)

In the simplest models of spray combustion it is assumed that the droplets burn individually according to the "d^2-law." Both theory and experiment show that this model only will be valid if the spray is extremely dilute, otherwise the droplets burn collectively in what is known as the group combustion mode. Most of work on spherical droplet cloud is limited to monodisperse sprays; however it is important to determine how the particle size distribution will affect group combustion, particularly the sheath combustion mode. In order to gain preliminary indication of the effect of the droplet size distribution of the vaporization process, the behavior of spays with a bimodal droplet size distribution is examined. The present study shows that for a cloud which is initially in saturated equilibrium the droplet size distribution changes the profiles of temperature and fuel vapor mass fraction within the vaporization wave at the edge of the cloud; however, the size distribution does not affect the overall evaporation characteristics such as the vaporization rate and the cloud lifetime in the sheath combustion limit considered here. It is shown that as before the cloud radius decreases according to a "d^2-law" with a modified vaporization constant.

Key Words: Droplet, Spray, Evaporation, Vaporization, Combustion, Group Combustion, Sheath Combustion. Fuel, Size Distribution, Cloud, Bimodal, Flame

NOMENCLATURE

a : Droplet radius
c_p : Specific heat of the mixtures
d : Droplet diameter
D : Mass diffusion coefficient
G : Gas constant
L : Latent heat of vaporization
$\dot{m}$: Vaporization rate per unit volume of cloud
M : Molar concentration of species
n : Number density on the liquid droplets
p : Total pressure
r : Radial coordinate
R : Cloud radius
t : Time
T : Temperature
u : Internal energy
U : Vaporization speed
v : Gas phase velocity
W_f : Fuel molecular weight
W_o : Oxidizer molecular weight
α : Thermal diffusivity of the gas phase, $\alpha=\lambda/\rho_g c_p$
δ : $(4\pi(\beta n_1 a_{1i}+n_2 a_{2i}))^{-1/2}$, Order of wave thickness
λ : Gas phase thermal conductivity
ρ : Density
τ_c : Cloud lifetime
$\bar{a}_1$: a_1/a_{1i}, Smaller dropler radius
$\bar{a}_2$: a_2/a_{2i}, Larger dropler radius
C : Edge temperature of the cloud
L_e : Lewis number, $L_e=\alpha/D$
m_{1a} : Ratio of liquid to air mass, $m_{1a}=m_{1i}/m_{ai}$
m_{12} : Ratio of smaller to larger droplet mass, $m_{12}=m_{1i}/m_{2i}$
$\bar{r}$: r/R_i, Radial coordinate
$\bar{v}$: $v/(\alpha_1/R_i)$, Gas phase velocity
W : Ratio of the molecular weights of the non-condensible to vaporizing species
Y : $\hat{Y}_r-\hat{Y}$, Perturbation in fuel vapor mass fraction
$\hat{Y}$: Fuel vapor mass fraction
$\hat{Y}_o$: Oxidizer mass fraction
Z : Parameter, defined in Eq.(31)
β : a_{1i}^2/a_{2i}^2, Ratio of surface area of smaller to larger droplets
β_1 : $n_1 a_{1i}/n_2 a_{2i}$, Parameter
β_3 : $n_1 a_{1i}^3/n_2 a_{2i}^3$ or m_{12}
γ_0 : Eigenvalue in wave solution
$\bar{\rho}$: ρ/ρ_r, Gas phase density
ε : $[4\pi(\beta n_1 a_{1i}+n_2 a_{2i})R_i^2]^{-1/2}$, Parameter
θ : $c_p(T-T_r)/L$, Temperature variable
ξ : R/R_i, Dimensionless cloud radius
ϕ : $\bar{\rho}\bar{v}$, Mass flux
Δ : Vaporization wave thickness

Subscript

a : Air property
b : Region where all the smaller droplets are completely vaporized
av : Averaged condition
f : Liquid fuel property
g : Mixture gas
i : Initial state
l : Liquid property
r : Reference condition
s : Droplet surface
v : Vapor
∞ : Ambient condition

*Korea Institute of Nuclear Safety, P.O.Box 7, Daeduk-Danji. Daejon 305-606, Korea

0,1,2,… : Solution orders
1 : Smaller droplet
2 : Larger droplet
c : Cloud interior
e : Cloud edge
i : Inner cloud region
o : Outer cloud region
w : Wave

1. INTRODUCTION

In the practical combustion of the liquid fuel sprays, dense droplet sprays prevail and conditions experienced by discrete droplets may be quite different from those obtained in single dropler analysis, notably due to droplet interactions. Recently, the flame surrounds the entire spray and there is no evidence of separate flames surrounding individual droplets.

Chigier and McCreath (1973, 1974) observed dense liquid sprays with flame fronts at the periphery of the spray sheath and suggested that the flame fronts are at such great distances from the droplet surfaces that diffusion of heat and mass is governed by turbulent diffusion as well as by temperature and concentration gradients across the spray sheath. Chiu et al (1971, 1977, 1982) have developed a series of group combustion models for the structure and burning characteristics of liquid fuel sprays. The collective behavior of the droplets is taken into account by a simultaneous analysis of an inner heterogeneous region and an outer homogeneous gas-phase region. Spray combustion models are classified according to a group combustion number G. Labowsky and Rosner(1978) have found similar results. A different terminology was used: their "incipient group combustion" is internal group combustion and their "total group combustion" is external group combustion. A quasi-steady continuum approach was used similar to that of Chiu and co-workers, and a superposition method with discrete monopole sources was used in developing the theory. It was shown that the Thiele Modulus Ψ is an important parameter in the determination of the onset of intermal group combustion.

Correa and Sichel(1982a, 1982b) performed an asymptotic analysis for small ε_1 values and obtained external sheath combustion results that agree well with those of Chiu and co-workers. Where $\varepsilon_1=(4\pi n a_i R_i^2)^{-1}$ is the square of the ratio of the two lengths $(4\pi n a_i)^{-1/2}$ and R_i and $(4\pi n a_i)^{-1/2}$ is the order of the thickness of a vaporization wave at the edge of the cloud, R_i is the initial cloud radius. A d^2-law based on the cloud size is obtained in this quasi-steady sheath limit. In limiting cases $\varepsilon_1 \ll 1$ droplet evaporation only occurs across a thin front or vaporization wave of thickness Δ at the edge of the cloud. The interior of the cloud remains in undisturbed saturated equilibrium and combustion occurs at a diffusion flame sheet outside the cloud analogous to single droplet burning. It is readily shown that the parameter $\varepsilon_1 \sim (\Delta/R_i)^2$. This mode of burning, which is somtimes referred to as sheath combustion, is illustrated in Fig. 1. These three parameters, although derived differently, can be shown to be closely related. Sichel and Palaniswamy (1984) indicated that both the group combustion number G and Thiele Modulus Ψ can be expressed in terms of ε_1 so that with $Le=1$ and $Re=0$,

$$G=\Psi^2=\varepsilon_1^{-1}$$

Most of the work on spherical droplet cloud is limited to

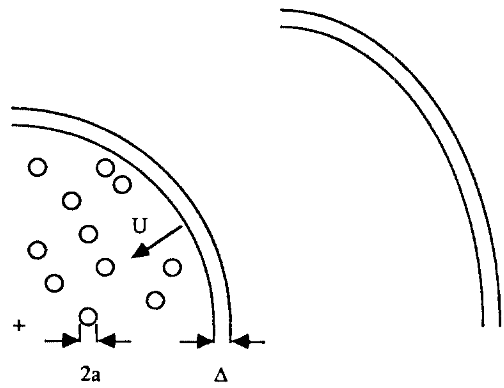

Fig. 1 Sheath combustion mode

monodisperse sprays. However, a knowledge on the behavior of clouds with generalized droplet size distribution may be important in determining the cloud lifetime and other vaporization or burning characterictics. Due to the difficulties in utilizing the distribution functions, a simple bimodal droplet size distribution has been assumed in the study presented here to qualitatively investigate the effect of the size distribution on spray clouds.

The behavior of bimodal cloud in the present study is an extention of the analysis of the behavior of an quiescent, spherically symmetrical, uniform and monodisperse cloud of single component fuel droplets undergoing pure vaporization or burning in an prescribed ambient atmosphere established by Correa and Sichel (1982a, 1982b). As in the analysis of Corra and Sichel (1982a, 1982b) a vaporization wave is found to propagate into the cloud interior. The structrue of this wave, which does depend on the size distribution as well as on parameters such as the liquid-air mass ratio and the initial cloud radius for the vaporizing cloud have been determined as described in detail below.

For the purely vaporizing case, the present study shows that the bimodal droplet size distribution does not affect the cloud lifetime.

2. A PURELY-VAPORIZING CLOUD WITH A BIMODAL DROPLET SIZE DISTRIBUTION

A spherical cloud with a bimodal droplet size distribution in a quiescent atmosphere is considered. The cloud has an initial radius R_i and contains both smaller droplets of initial radius a_{1i} with number density n_1 and larger droplets of initial radius a_{2i} with number density n_2. Then the ratios m_{12} which is defined as $n_1 a_{1i}^3/n_2 a_{2i}^3$ and m_{1a} which is defined as $\frac{\rho_l}{\rho_{ai}}\frac{3}{4}\pi(n_1 a_{1i}^3+n_2 a_{2i}^3)$ will be important parameters in this analysis. The following assumptions have been made in the analysis:

(1) The cloud is initially in saturated equilibrium at a certain reference temperature T_r and the droplet temperature is assumed to remain constant at this value during the vaporization process.

(2) The details of the initial heat-up processes during which the cloud interior reaches saturated equilibrium are not

considered. Thus only the gas-phase equations within and outside the cloud need to be considered with the liquid phase treated as a continuous mass source and energy sink.

(3) Since only a binary mixture of a fuel vapor and oxidizer is considered, Fick's law of diffusion is valid.

(4) The pressure is constant everywhere.

(5) The Lewis number Le is taken to be unity.

(6) The effect of droplet interactions is negligible.

(7) Both smaller and larger droplets are uniformly distributed.

Following Williams(1965), the conservation equations of mass, species and energy for this spherically symmetric system are as follows:

$$\frac{\partial \rho}{\partial t}+\frac{1}{r^2}\frac{\partial}{\partial r}[r^2\rho v]=\begin{cases}\dot{m}, \text{ inside the cloud}\\ 0, \text{ outside the cloud}\end{cases} \tag{1}$$

$$\frac{\partial}{\partial t}(\rho\hat{Y})+\frac{1}{r^2}\frac{\partial}{\partial r}\left[r^2\left\{\rho v\hat{Y}-\rho D\frac{\partial \hat{Y}}{\partial r}\right\}\right]=\begin{cases}\dot{m}\\ 0\end{cases} \tag{2}$$

$$\frac{\partial}{\partial t}(\rho u)+\frac{1}{r^2}\frac{\partial}{\partial r}\left[r^2\left\{\rho v c_p(T-T_r)-\lambda\frac{\partial T}{\partial r}\right\}\right]=\begin{cases}-\dot{m}L\\ 0\end{cases} \tag{3}$$

The vaporization rate per unit volume of the cloud is obtatined by summing the vaporization rate of the smaller and larger droplets and is given by:

$$\begin{aligned}\dot{m}&=-4\pi\rho_l\left[n_1a_1^2\frac{\partial a_1}{\partial t}+n_2a_2^2\frac{\partial a_2}{\partial t}\right]\\ &=\frac{4\pi\lambda}{c_p}[n_1a_1+n_2a_2]\ln\left[1+\frac{c_p(T-T_r)}{L}\right]\end{aligned} \tag{4}$$

Equation (4) is obtained from the standard quasi-steady single droplet theory using the local cloud conditions as the ambient conditions for each droplet. All symbols are defined in the Nomenclature.

2.1 Analysis of the Cloud Edge and Interior

The conservation Eqs.(1, 2, 3) and the relation for the vaporization rate per unit volume of the cloud, equation (4) may be non-dimensionalized with the characteristic length R_i, velocity α_r/R_i, and time R_i^2/α_r. This corresponds to the scheme used by Correa and Sichel(1982a). Then it follows that within the cloud:

$$\varepsilon\frac{\partial\bar{\rho}}{\partial\bar{t}}+\frac{\varepsilon}{\bar{r}^2}\frac{\partial}{\partial\bar{r}}[\bar{r}^2\bar{\rho}\bar{v}]=\frac{\beta_1\bar{a}_1+\bar{a}_2}{1+\beta_3}\ln(1+\theta) \tag{5}$$

$$\varepsilon\frac{\partial}{\partial\bar{t}}\{(\bar{\rho}(Y_r-Y)\}+\frac{\varepsilon}{\bar{r}^2}\frac{\partial}{\partial\bar{r}}\left[\bar{r}^2\left\{\bar{\rho}\bar{v}(Y_r-Y)+\frac{\partial Y}{\partial\bar{r}}\right\}\right]=\frac{\beta_1\bar{a}_1+\bar{a}_2}{1+\beta_3}\ln(1+\theta) \tag{6}$$

$$\varepsilon\frac{\partial}{\partial\bar{r}}\{\bar{\rho}\bar{u}\}+\frac{\varepsilon}{\bar{r}^2}\frac{\partial}{\partial\bar{r}}\left[\bar{r}^2\left\{\bar{\rho}\bar{v}\theta-\frac{\partial\theta}{\partial\bar{r}}\right\}\right]=-\frac{\beta_1\bar{a}_1+\bar{a}_2}{1+\beta_3}\ln(1+\theta) \tag{7}$$

$$\frac{\partial\bar{a}_1^2}{\partial\bar{t}}=-2\frac{R_i^2}{a_{1i}^2}\frac{\rho_r}{\rho_l}\ln(1+\theta) \tag{8}$$

$$\frac{\partial\bar{a}_2^2}{\partial\bar{t}}=-2\frac{R_i^2}{a_{2i}^2}\frac{\rho_r}{\rho_l}\ln(1+\theta) \tag{9}$$

A significant result is that the group combustion parameter ε_1 is replaced by the composite small parameter

$$\varepsilon=[4\pi(\beta n_1a_{1i}+n_2a_{2i})R_i^2]^{-1}$$
$$\text{with } \beta=a_{1i}^2/a_{2i}^2 \tag{10}$$

Since the parameter ε is much less than 1 in typical sprays, the highest-order derivatives in Eqs.(1, 2, 3) are multiplied by the small parameter ε suggesting the possibility of the existence of a boundary-layer as is typical of singular perturbation problems. Substituting the straight forward expansions of the variables into the goverming equations, it is easily found that there must be a singular region or boundary layer at the edge of the cloud where the highest order (conduction, diffusion) terms neglected in the zeroth order solution become important due to the steepness of the spatial derivatives. θ^e, temperature at the edge of the cloud is positive only within this layer where all of the vaporization occurs. The cloud radius will decrease as the outermost droplets vaporize, while the interior of the cloud will remain in saturated equilibrium.

Also assuming that the vaporization front or wave at the edge of the cloud has a thickness of order $\varepsilon^\nu R_i$, where ν is as yet unknown, the following stretched inner variables are now introduced to describe the flow within the wave

$$\begin{aligned}&r^w=(R-r)/R_i\varepsilon^\nu,\quad r<R_i\\ &t^w=t/(R_i/U_r)\end{aligned} \tag{11}$$

where $R=R_i-\mathrm{U}t$ and the wave-fixed coordinates are used to shift the singular boundary conditions to the origin of the inner coordinates.

The inner variables are now as follows:

$$\begin{aligned}&\bar{v}=-v^w=-[v_o^w+\varepsilon^\nu v_1^w+\varepsilon^{2\nu}\{v_2^w+R_iU_o/\alpha_r\}+\cdots\cdots\\ &\theta=\theta^w=\varepsilon^\nu\theta_o^w+\varepsilon^{2\nu}\theta_1^w+\cdots\cdots\\ &\bar{a}_1=a_1^w=a_{1o}^w+\varepsilon^\nu a_{11}^w+\cdots\cdots\\ &\bar{a}_2=a_2^w=a_{2o}^w+\varepsilon^\nu a_{21}^w+\cdots\cdots\\ &Y=Y^w=\varepsilon^\nu Y_o^w+\varepsilon^{2\nu}Y_1^w+\cdots\cdots\\ &\bar{p}=p^w=p_o^w+\varepsilon^\nu p_1^w+\cdots\cdots\\ &U=\varepsilon^{2\nu}U_o+\varepsilon^{3\nu}U_1+\cdots\cdots\end{aligned} \tag{12}$$

where $U>0$ is the speed at which the layer or wave moves into the cloud and the term $\varepsilon^{2\nu}R_iU_o/\alpha_r$ is an apparent convection speed due to the use of wave-fixed coordinates. With the substitution of the expansions (12) into Eqs.(5, 6, 7, 8, 9) the unknown ν must be $1/2$ in order that the derivative terms in Eqs.(5)~(9) be balanced with the evaporative source terms. Then the wave thickness will be of the order of $R_i\,\varepsilon^{1/2}$, i.e., of the order of$(4\pi(\beta n_1a_{1i}+n_2a_{2i}))^{-1/2}$.

Vaporization occurs across a thin vaporization wave at the edge of the cloud. However, for sprays with a bimodal droplet size distribution the smaller droplets evaporate much faster than the larger droplets due to the higher surface to volume ratio; thus only the larger droplets remain near the edge of the cloud region, $0\le r^w\le r_b^w$, while both large and small droplets will be present in the inner region, $r_b^w\le r^w\le\infty$, as shown in Fig. 2. The wave structure is governed by two

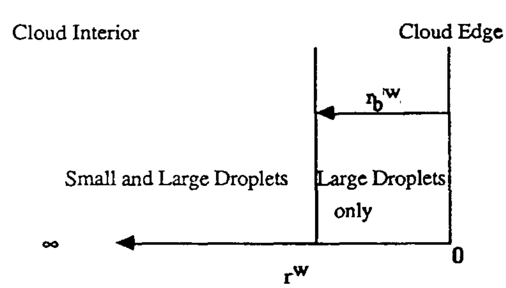

Fig. 2 Vaporization wave structure of bimodal sprays

different sets of equations for each of these regions.

For sprays with a bimodal droplet size distribution, the smaller droplets evaporate much faster than the larger droplets due to the higher surface to volume ratio; thus there will be two regions, one in which all the smaller droplets are completely evaporated, $0 \le r^w \le r_b^w$, and a second in which both smaller and larger droplets exist jointly, $r_b^w \le r^w \le \infty$, as shown in Fig. 2. With the substitution of Eq.(12) and the Galilean Transformation Eq.(11), Eqs.(5, 6, 7, 8, 9) will be divided into two regions, to lowest order, as follows:

(a) region **1**:$0 \le r^w \le r_b^w$(only larger droplets exist)

$$\frac{d\phi_o^w}{dr^w} = \frac{a_{2o}^w}{1+\beta_3}\theta_o^w \tag{13}$$

$$\frac{d}{dr^w}\left\{\phi_o^w Y_r + \frac{dY_o^w}{dr^w}\right\} = \frac{a_{2o}^w}{1+\beta_3}\theta_o^w \tag{14}$$

$$\frac{d}{dr^w}\left\{\frac{d\theta_o^w}{dr^w}\right\} = \frac{a_{2o}^w}{1+\beta_3}\theta_o^w \tag{15}$$

$$(a_{1o}^w) = 0 \tag{16}$$

$$\frac{d(a_{2o}^w)^2}{dr^w} = \gamma_o\theta_o^w \tag{17}$$

(b) region 2 : $r_b^w \le r^w \le \infty$(both smaller and larger droplets exist)

$$\frac{d\phi_o^w}{dr^w} = \frac{\beta_1 a_{1o}^w + a_{2o}^w}{1+\beta_3}\theta_o^w \tag{13a}$$

$$\frac{d}{dr^w}\left\{\phi_o^w Y_r + \frac{dY_o^w}{dr^w}\right\} = \frac{\beta_1 a_{1o}^w + a_{2o}^w}{1+\beta_3}\theta_o^w \tag{14a}$$

$$\frac{d}{dr^w}\left\{\frac{d\theta_o^w}{dr^w}\right\} = \frac{\beta_1 a_{1o}^w + a_{2o}^w}{1+\beta_3}\theta_o^w \tag{15a}$$

$$\frac{d(a_{1o}^w)^2}{dr^w} = \frac{1}{\beta}\gamma_o\theta_o^w \tag{16a}$$

$$\frac{d(a_{2o}^w)^2}{dr^w} = \gamma_o\theta_o^w \tag{17}$$

where $\phi_o^w = \rho_o^w v_o^w$, $\beta_1 = n_1 a_{1i}/n_2 a_{2i}$, $\beta_3 = n_1 a_{1i}^3/n^2 a_{2i}^3$ where β_3 represents the ratio of the smaller to the larger droplet mass, and the region $r^w \le r_b^w$ represents the ratio of the smaller to the larger droplet mass, and the region $r^w \le r_b^w$ represents the region near the edge of the cloud where all the smaller droplets are completely vaporized.

The parameter γ_o, which is given by:

$$\gamma_o = \frac{2R_i\lambda}{a_{2i}^2\rho_1 c_p U_o} \tag{18}$$

plays the role of an eigenvalue which determines the propagation speed U_o of the wave.

Boundary conditions at the cloud edge may be obtained from the conservation of mass, species and energy across the wave as described in Appendix.

At the cloud edge($r^w = 0$) vaporization is just complete so that

$$a_{1o}^w(0) = 0,\ a_{2o}^w(0) = 0 \tag{19}$$

From conservation of mass across the wave

$$\phi_o^w(0) = -\frac{1}{\gamma_o}\left\{\frac{2}{3} + \frac{\rho_r/\rho_1}{2\pi(n_1 a_{1i}^3 + n^2 a_{2i}^3)}\right\} \tag{20}$$

From conservation of fuel species across the wave

$$\left.\frac{dY_o^w}{dr^w}\right|_{r^w=0} = -\frac{2}{3\gamma_o}(1-Y_r) \tag{21}$$

From conservation of energy across the wave

$$\left.\frac{d\theta_o^w}{dr^w}\right|_{r^w=0} = -\frac{2}{3\gamma_o} \tag{22}$$

Also the boundary conditions at $r^w = r_b^w$ becomes

$$a_{1o}^w = 0,\ a_{2o}^w = a_b^w,\ \theta_o^w = \theta_{ob}^w,\ Y_o^w = Y_{ob}^w \tag{23}$$

If it is assumed that the evaporation of the individual droplets follows the "d^2-law", and if the time rate of change of square of the droplet radius is the same for both smaller and larger droplets(i.e., equal evaporation constant), the radius of the larger droplets at $r^w = r_b^w$, a_b^w, can be expressed as

$$a_b^{w2} = 1 - (a_{1i}^2/a_{2i}^2) = 1 - \beta \tag{24}$$

The interior of the cloud is approached as $r^w \to \infty (\varepsilon \to 0$, fixed $\bar{r}$); thus

as $r^w \to \infty$: $a_{1o}^w \to a_{2o}^w \to 1,\ \theta_o^w \to 0,\ Y_o^w \to 0$

$$\phi_o^w \to \frac{\rho_r/\rho_1}{2\pi\gamma_o(n_1 a_{1i}^3 + n_2 a_{2i}^3)} \tag{25}$$

This convective flux represents the flow from the cloud interior as seen in wave-fixed coordinates. An arbitrary edge-temperature will now be introduced in order to establish the nature of wave structure; the actual edge temperature will be obtained later from an analysis of the region outside the cloud. Thus it is assumed that

$$\theta_o^w(0) = C \tag{26}$$

Solutions of the vaporization wave structure can be obtained approximately, exactly, or numerically where required.

(1) Approximate Solutions

a_{1o}^w and a_{2o}^w can be eliminated from the energy and droplet evaporation equations Eqs.(15, 16, 16a, 17) for the limiting condition $\beta_1 \ll 1$ implying relatively few smaller droplets. Then the resulting approximate equation for θ_o^w yields for both regions:

$$\frac{d^3\theta_o^w}{dr^{w3}}\theta_o^w - \frac{d^2\theta_o^w}{dr^{w2}}\frac{d\theta_o^w}{dr^w} = 0 \tag{27}$$

Applying the boundary conditions Eqs.(19, 20, 21, 22, 23, 24, 25, 26) the results are summarized as follows:

$$\theta_o^w = C\exp\left[-\frac{2}{3\gamma_o}\frac{r^w}{C}\right]$$

$$\begin{aligned}
(a_{1o}^w)^2 &= 0 && \text{for } 0 \le r^w \le r_b^w \\
&= 1 - \frac{3}{2\beta}\gamma_o^2 C^2 \exp\left[-\frac{2}{3\gamma_o}\frac{r^w}{C}\right] && \text{for } r_b^w \le r^w \le \infty \\
(a_{2o}^w)^2 &= \frac{3}{2}\gamma_o^2 C^2\left\{1 - \exp\left[-\frac{2}{3\gamma_o}\frac{r^w}{C}\right]\right\} && \text{for } 0 \le r^w \le r_b^w \\
&= 1 - \frac{3}{2}\gamma_o^2 C^2 \exp\left[-\frac{2}{3\gamma_o}\frac{r^w}{C}\right] && \text{for } r_b^w \le r^w \le \infty
\end{aligned}$$

$$\phi_o^w = -\frac{1}{\gamma_o}\left\{\frac{2}{3}\exp\left[-\frac{2}{3\gamma_o}\frac{r^w}{C}\right] + \frac{\rho_r/\rho_1}{2\pi(n_1 a_{1i}^3 + n_2 a_{2i}^3)}\right\}$$

$$Y_o^w = C(1-Y_r)\exp\left[-\frac{2}{3\gamma_o}\frac{r^w}{C}\right]$$

and

$$\gamma_o C = \sqrt{(2/3)} \tag{28}$$
$$\theta_{ob}^w / C = 1 - a_b^{w2} \tag{29}$$
$$r_b^w = -\sqrt{(3/2)} \ln(\theta_{ob}^w / C) \tag{30}$$

It should be noted that $\gamma_o C$, θ_{ob}^w/C, and r_b^w do not depend on the ratio of the smaller to the larger droplets mass m_{12} or the ratio of the liquid to the air mass m_{la} for $\beta_1 \ll 1$. Approximate analytical solutions are no longer possible when $\beta_1 \sim O(1)$, and solutions must then be determined numerically as described below.

(2) Exact Relations Between Vaporization Wave Parameters

By defining $Q = d\theta_o^w/dr^w$ the temperature θ_o^w can be expressed in terms of γ_o and the larger droplet radius a_{2o}^w, and an exact relationship between γ_o and $\theta_o^w(0)$ can be obtained.

for $0 \le r^w \le r_b^w$

$$\theta_o^{w2} = \frac{4}{3\gamma_o^2(1+\beta_3)} \left\{ \frac{2}{5} a_{2o}^{w5} - (1+\beta_3) a_{2o}^{w2} \right\} + \theta_o^w(0)^2$$

for $r_b^w \le r^w \le \infty$

$$\theta_o^{w2} = -\{\beta_1(a1_o^{w5-1}) + (a_{2o}^{w5-1}) + \frac{1-a_{2o}^{w2}}{1-a_b^{w2}} \left\{ \frac{15\gamma_o^2(1+\beta_3)\theta_{ob}^{w2}}{4} + 1 - a_b^{w5} \right\} \}$$

These equations may be used at $r^w = r_b^w$ to obtain the exact relation

$$\gamma_o^2 = Z / \{\theta_o^w(0)^2 - \theta_{ob}^{w2}\} \tag{31}$$

where $Z = -\frac{4}{3(1+\beta_3)} \left\{ \frac{2}{5} a_b^{w5} - (1+\beta_3) a_b^{w2} \right\}$

(3) Numerical Solutions

The approximate solutions developed above provide results which are valid only for the limited condition $\beta_1 \ll 1$, while the exact relationships between γ_o and $\theta_o^w(0)$ give expressions in terms of θ_{ob}^w which is unknown at this stage. Thus Eqs. (13, 14, 15, 16, 17) have been integrated numerically to evaluate the parameters $\gamma_o C$, θ_{ob}^w/C, and r_b^w for a given β_3 and to check the accuracy of the approximate analytical solutions. To integrate these equations the direct step by step integration was initiated from $r^w = 0$ with an assumed value of the eigenvalue γ_o. The final solution was then be obtained by guessing values of the eigenvalue until the correct value satisfying the matching conditions within the cloud as given by Eq.(25) was determined.

Results obtained for various values of β_3 are shown in Table 1 below, which also includes results from the approximate analysis. The results are expressed in terms of $\gamma_o C$, θ_{ob}^w/C can only be determined after the temperature distribution outside the cloud has been determined. It can be seen that the eigenvalue $\gamma_o C$ is not very sensitive to m_{12}; however, θ_{ob}^w/C, the ratio of the temperature at $r^w = r_b^w$ to the edge temperature of the cloud, increases as m_{12} increases, and r_b^w which represents the thickness of the region in which only larger droplets are present decreases with increasing m_{12} as is to be expected. Agreement between the approximate and numerical solutions is only fair.

Table 1 Comparison of approximate and numerical results for various values of β_3 or m_{12}

$\beta_3(=m_{12})$	$\gamma_o C$		θ_{ob}^w/C		r_b^w	
	Approx	Numeric	Approx	Numeric	Approx	Numeric
0.0	0.816	0.894				
0.001	0.816	0.895	0.01	0.024	5.64	4.60
0.01	0.816	0.897	0.01	0.030	5.64	4.30
0.1		0.922		0.058		2.95
1.0		1.031		0.061		2.00
2.0		1.073		0.069		1.85
5.0		1.113		0.075		1.70

Results have been obtained for a bimodal cloud with 10μm amd 100μm octane droplets at an ambient temperature 500°K and an ambient oxidizer mass fraction 0.23. A typical example of the structure of the vaporization wave of octane cloud for $m_{12}=0.01$ and $m_{la}=4.25$ is shown in Fig. 3. It is clearly shown that the temperature and concentration gradients are very steep near the cloud edge and approach zero toward the

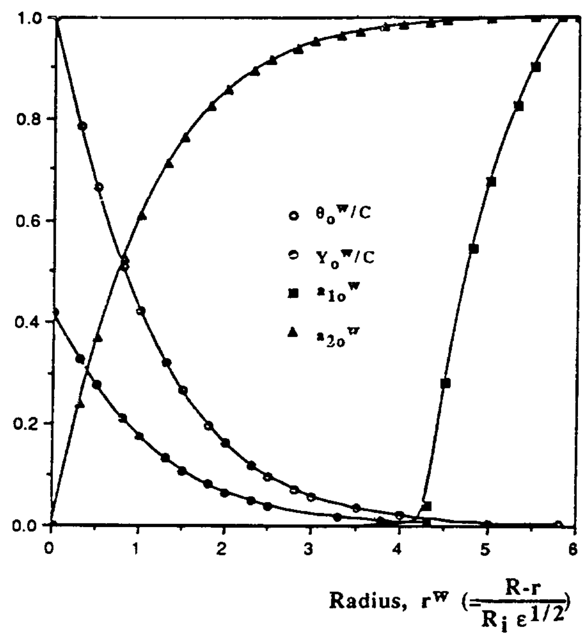

Fig. 3 Structure of vaporization wave for $m_{12}=0.01$ (for octane cloud, Table 2)

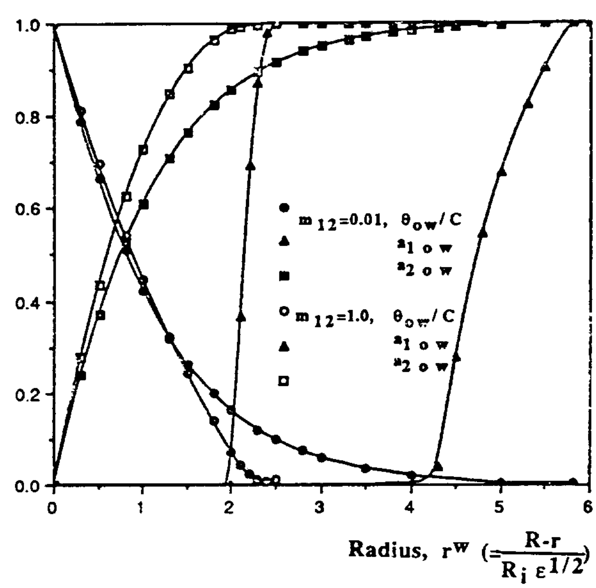

Fig. 4 Effect of m_{12} in vaporizing Cloud for $m_{12}=4.25$ (for octane cloud, Table 2)

cloud interior, and both smaller and larger droplets are completely evaporated at the edge of the cloud and approach saturation conditions at the cloud interior. Also Fig. 4 shows the structrue of the vaporization wave inside the cloud for $m_{12}=0.01$ and 1.0, which is obtained from the numerical calculation. For bimodal sprays smaller droplets evaporate faster than larger droplets because of the higher surface to volume ratio. Thus as the ratio of the mass of the smaller to the larger droplets m_{12} increases, the evaporation rate of the larger droplets at the cloud edge is smaller and r_b^w, where all the smaller droplets are completely vaporized, is closer to the edge of the cloud.

2.2 Analysis of the Region Outside the Cloud

The analysis of the region inside the cloud provided information on the profiles of temperature and fuel vapor mass fraction only in terms of θ_o^w/C and Y_o^w/C. In order to complete the solution and determine $\theta_o^w(0)$, the temperature at the edge of the cloud, it now becomes necessary to determine a solution for the region outside the cloud.

This region contains no droplets and is governed by Eqs.(1, 2, 3) without source terms. The Eqs.(1, 2, 3) may be nondimensionlized with the characteristic length R_i, velocity a_r/R_i, and time R_i/U_r, where $U_r=\varepsilon U$ or is reference vaporization wave speed. The dimensionless equations to zeroth order in the inner region follow below:

$$\frac{d}{d\bar{r}}[\bar{r}^2\rho_o^i v_o^i]=0 \tag{32}$$

$$\rho_o^i v_o^i\frac{dY_o^i}{dr}=\frac{1}{\bar{r}^2}\frac{d}{d\bar{r}}\left[\bar{r}^2\frac{dY_o^i}{d\bar{r}}\right] \tag{33}$$

$$\rho_o^i v_o^i\frac{d\theta_o^i}{d\bar{r}}=\frac{1}{\bar{r}^2}\frac{d}{d\bar{r}}\left[\bar{r}^2\frac{d\theta_o^i}{d\bar{r}}\right] \tag{34}$$

The analysis below is similar to that presented by Correa and Sichel(1982a), but is modified by the changed boundary conditions at the vaporization wave surface. From the vaporization wave analysis it follows that the zeroth order boundary conditions at the cloud edge where $\bar{r}=\zeta=R/R_i$ are:

$$\rho_o^i v_o^i=\frac{2}{3\gamma_o} \tag{35}$$

$$Y_o^i=0,\quad \frac{dY_o^i}{d\bar{r}}=\frac{2}{3\gamma_o}(1-Y_r) \tag{36}$$

$$\theta_o^i=0,\quad \frac{d\theta_o^i}{d\bar{r}}=\frac{2}{3\gamma_o} \tag{37}$$

while matching with the zeroth order outer solution which are constatn amibient conditions gives to lowest oreder as $r\to\infty$

$$\begin{aligned}&\theta_o^i\to\theta_\infty\\ &Y_o^i\to\hat{Y}_r-\hat{Y}_\infty\\ &v_o^i\to 0\end{aligned} \tag{38}$$

Then the profiles of the fuel vapor mass fraction and temperature outside the cloud become, respectively:

$$Y_o^i=(1-\hat{Y}_r)e^{K/\zeta-K/\bar{r}}-(1-\hat{Y}_r) \tag{39}$$

$$\theta_o^i\to e^{K/\zeta-K/\bar{r}}-1 \tag{40}$$

It is now possible to relate the eigenvalue γ_o and other parameters within the bimodal cloud to ambient conditions outside the cloud. For this purpose it is also necessary to use the relation below between γ_o and other parameters which was obtained earlier:

$$\begin{aligned}\gamma_o^2&=-\frac{4}{3(1+\beta_3)}\{\frac{2}{5}a_b^{w5}-(1+\beta_3)a_b^{w2}\}\frac{1}{\{\theta_o e^2-\theta_{ob}w^2\}}\\ &=Z/\{\theta_o e^2-\theta_{ob}w^2\}\end{aligned} \tag{31}$$

where $Z=-\frac{4}{3(1+\beta_3)}\{\frac{2}{5}a_b w^5-(1+\beta_3)a_b w^2\}$,
and $\theta_o^e=\theta_o^w(0)$

And the results can be summarized as follows:

$$\begin{aligned}U_o&=\frac{3R_i\lambda}{a_{2i}^2\rho_l c_p}\,\frac{\ln(1+\theta_\infty)}{\xi}\\ &=\frac{2R_i\lambda}{a_{2i}^2\rho_l c_p}\,(\frac{\theta_o^{e2}-\theta_{ob}^{w2}}{Z})^{1/2}\end{aligned} \tag{41}$$

$$\begin{aligned}\frac{d\xi^2}{dt}&=-\frac{6\varepsilon\lambda}{a_{2i}^2\rho_l c_p}\ln(1+\theta_\infty)\\ &=\frac{6\varepsilon\lambda}{a_{2i}^2\rho_l c_p}\ln\,(1+\frac{c_p(T_\infty-T_r)}{L})\end{aligned} \tag{42}$$

$$\text{and}\quad \xi^2=1-t/\tau_c \tag{43}$$

where the cloud lifetime τ_c is given by

$$\begin{aligned}\tau_c&=\frac{a_{2i}^2\rho_l c_p}{6\varepsilon\lambda\,\ln\,(1+\theta_\infty)}\\ &=\frac{2\pi(n_1 a_{1i}^3+n_2 a_{2i}^3)R_i^2\rho_l\,c_p}{3\lambda\,\ln(1+\theta_\infty)}\end{aligned} \tag{44}$$

Equation (43) shows that the cloud with a bimodal spray also obeys a "d^2-law"like the monodisperse cloud. It should be noted that the cloud lifetime for monodisperse spray obtained by Correa ans Sichel (1984) is easily recovered from Eq. (44) for either $n_1=0$ or $n_2=0$. If, as in most cases of interest, the initial volume of liquid droplets per unit volume $4/3\pi(n_1\,a_{1i}^3+n_2 a_{2i}^3)\ll 1$, the ratio of the initial mass of the liquid to the air m_{la} becomes

$$\begin{aligned}m_{la}&=\frac{\rho_l}{\rho_{ai}}\,\frac{4}{3}\pi(n_1 a_{1i}^3+n_2 a_{2i}^3)\\ &=\frac{\rho_l}{\rho_{ai}}\frac{a_{2i}^2}{R_i^2}\frac{1}{3\varepsilon}\end{aligned} \tag{45}$$

and the cloud lifetie τ_c becomes

$$\tau_c=\frac{m_{la}\rho_{ai}C_p R_i^2}{2\lambda\,\ln\,(1+\theta_\infty)} \tag{46}$$

$$\text{or}\ =\frac{\rho_f C_p R_i^2}{2\lambda\,\ln(1+\theta_\infty)} \tag{47}$$

wherer $\rho_f=m_{la}\rho_{ai}$ is the liquid mass per unit volume of spray. This result is identical to that obtained by Correa and Sichel (1982a) and shows that the cloud lifetime depends only on the mass ratio m_{la} or ρ_f and does not depend on the mass loading ratio m_{12}. The effect of the mass ratio m_{la} on cloud lifetime is shown in Fig. 5 for octane cloud described in Table 2 below. As the liquid-air mass ratio is increased cloud lifetime increases, the wave speed decreases and the wave thickness, which is discussed below, increases.

Finally, the temperature θ^e at the edge of the cloud becomes

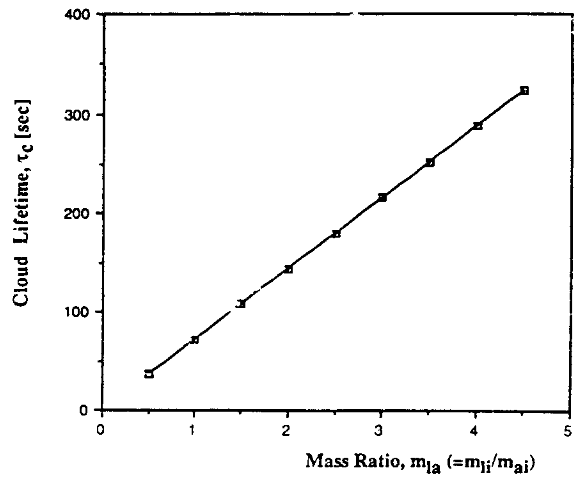

Fig. 5 Effect of mass ratio m_{1a} on cloud lifetime (for octane cloud, Table 2)

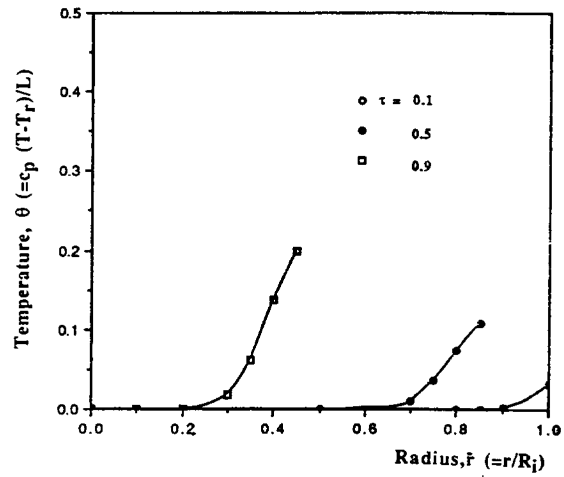

Fig. 6 Temperature profiles in vaporizing cloud for $m_{1a}=4.25$ ($\tau=t/\theta_c$, for octane cloud, table 2)

$$\theta^e=\varepsilon\theta_o^e+\cdots\cdots$$

$$=\left[\frac{Z\{\ln(1+\theta_\infty)\}^2}{1-t/\tau_c}+\theta_{ob}+\theta_{ob}{}^{W^2}\right]^{1/2} \tag{48}$$

The temperature profiles within the cloud, for the condition shown in Table 2, at various stages of its lifetime are shown in Fig. 6. The decreasing radius of the cloud and increasing edge temperature are easily seem. The variation of the edge temperature at $\tau=t/\tau_c=0.1$ for various values of m_{12}. However, it should be noted that the values of the edge temperature are extremely small compared with those outside the cloud. The temperature profiles outside the cloud at various stages of its lifetime are shown in Fig. 8.

The reference conditions in a saturated state, such as the temperature T_r, fuel vapor mass fraction $\hat{Y}_r$ and gas density ρ_r, respectively can be evaluated with the assumption that the interior of the cloud is saturated and is in thermodynamic equalibrium. Hence the relation between the temperature T_r and the fuel vapor mass fraction $\hat{Y}_r$, is given by the Clausius-Clapeyron relation:

$$\hat{Y}_r=\frac{1}{1-W+W\bar{P}\exp\{\frac{L}{G_f}(\frac{1}{T_b}-\frac{1}{T_r})\}} \tag{49}$$

where W is the ratio of the molecular weights of the non-

Table 2 Physical data for octane cloud

Cloud Parameters		
Intial cloud radius, R_i	0.1	[m]
Intial smaller droplet radius, a_{1i}	10	[μm]
Intial larger droplet radius, a_{2i}	100	[μm]
Mass ratio, m_{1a}	4.25	
Number density of smaller droplets, n_1	$0\sim10^{12}$	[m^{-3}]
Number densityu of larger droplets, n_2	$10^7\sim10^9$	[m^{-3}]
Liquid fuel density, ρ_l	707	[kgm^{-3}]
Liquid boiling temperature, T_b	398.7	[°K]
Latent heat of vaporization, L	300.1	[kJ/kg]
Vapor specific heat, cp	2.09	[kJ/kg °K]
Fuel molecuar weight, W_f	114.2	[kg/kg mol]
Oxidizer molecular weight, W_o	32	[kg/kg mol]
Thermal conductivity, λ	2.09×10^{-4}	[kJ/m sec °K]
Ambient Atemosphere Parameters		
Ambient temperatue, T_∞	500	[°K]
Ambient oxidizer mass fraction, $\hat{Y}_\infty$	0.23	

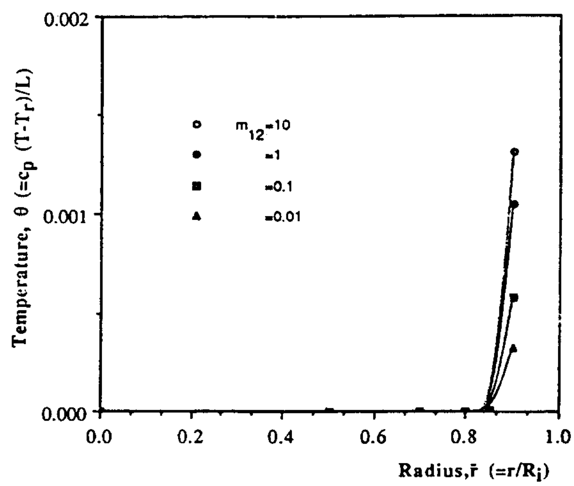

Fig. 7 Temperature profiles inside the cloud as a function of m_{12} at $t/\tau_c=0.1$(for octane cloud, Table 2)

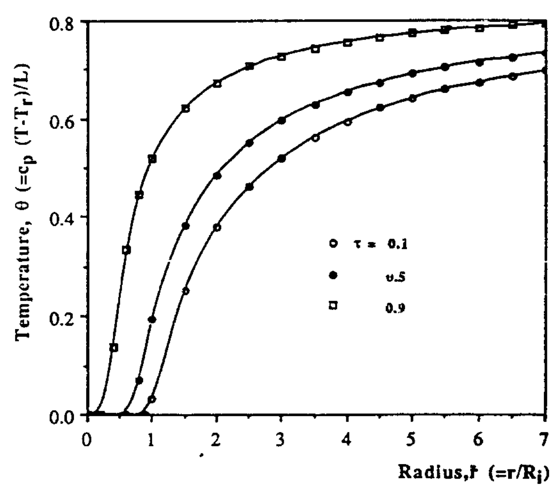

Fig. 8 Temperature profiles outside a vaporizing cloud for $m_{1a}=4.25$ and $\theta_\infty=1.00$ ($\tau=t/\tau_c$, for octane cloud, Table 2)

condensible to vaporizing species and $\bar{P}$ is the gas pressure in atm.

Also relation between the fuel vapor mass fraction and the temperature become

$$\theta_\infty = \frac{\hat{Y}_r - \hat{Y}_\infty}{1-\hat{Y}_r} = \frac{c_p(T_\infty - T_r)}{L} \tag{50}$$

and Eqs. (49, 50) are then sufficient to determine T_r and $\hat{Y}_r$.

As in the case of the monodisperse droplet cloud the behavior of lowest-order quasi-steady cloud with a bimodal droplet size distribution shows several analogies to single droplet theory. After cloud equilibrium is reached, the vaporization characteristics are determined not by the droplet size distribution but by the ratio of the initial mass of the liquid to air and by the initial air temperature. Thus if the mass ratio m_{la} is the same, the vaporization characteristics of bimodal sprays such as the cloud lifetime and the wave speed are the same as those of a monodisperse spray by Correa and Sichel (1982a).

This anlysis could be extended to evaluate the behavior of clous with generalized droplet size distribution fuctions. However it appears likely that size distribution will not affect the overall vaporization. The analysis could be continued as were done by Waldman (1974) or by Crespo and Linan (1975) to find the higher order solutions. These higher order solutions would show the effects of unsteadiness in the far field and introduce perturbations in the temperature at the cloud edge. However it were shown by Waldman (1974) or by Crespo and Linan (1975) that effect of the unsteadiness on the vaporization rate is small.

3. CONCLUSIONS

Evaporation of a spherical cloud with a bimodal droplet size distribution has been investigated in order to examine the effect of the droplet size distribution upon cloud behavior.

The lowest order quasi-steady cloud behavior for bimodal sprays in the sheath combustion limit shows that the cloud radius decreases according to a "d^2-law" analogous to the single droplet theory, although with a modified vaporization constant. The existence of an one-dimensional, quasi-steady vaporization wave which propagates radially into a vaporzing cloud was demonstrated for bimodal sprays.

The present study also shows that for a cloud which is initially in saturated equilibrium the droplet sise distribution changes the profiles of temperature and fuel vapor mass fraction within the vaporization wave at the edge of the cloud; however, the size distribution does not affect the overall evaporation characteristics such as the vaporization rate and the cloud lifetime in the sheath combustion limit considered here. The vaporization characteristics are determined not by the droplet size distribution but by the ratio of the initial mass of the liquid to air and by the initial air temperature.

This analysis could be extended to find higher order solutions in order to evaluate the effects of unsteadiness and be continued to evaluate the behavior of clouds with generalized droplet size distributions.

REFERENCES

Chigier, N.A. and McCreath, C.G., 1974, "Combustion of Droplets in Sprays", Acta Astronautica, Vol. 1, pp. 687~710.

Chiu, H. H. and Liu, T.M., 1977, "Group Combustion of Liquid Droplets", Combustion Science and Technology, Vol. 17, pp. 127~142.

Chiu, H.H., Kim, H.Y., and Croke, E.J., 1982, "Internal Group Combustion of Liquid Droplets", Nineteenth (Intl) Sym. on Combustion, The Combustion Institute, pp. 971~980.

Correa, S.M. and Sichel, M., 1982a, "The Boundary Layer Structure of a Vaporizing Fuel Cloud", Combustion Science and Technology, Vol. 28, pp. 121~130.

Correa, S.M. and Sichel, M., 1982b, "The Group Combustion of a Spherical Cloud of Monodisperse Fuel Droplets", Nineteenth (Intl) Sym. on Combustion, The Combustion Institute, pp. 981~991.

Crespo, A and Liñan, A., 1975, "Unsteady Effects in Droplet Evaporation and Combustion, Combustion Science and Technology Vol. 11, pp. 9~18.

Labowsky, M. and Rosner, D.E., 1978, "Group Combustion of Droplets in Fuel Clouds I. Quasi-Steady Predictions", Advances in Chemistry Series, No. 166, Amer. Chem. Soc., pp. 63~79.

McCreath, C.G. and Chigier, N.A., 1973, "Liquid Spray Burning in the Wake of Stabilized Disk,", Fourteenth (Intl.) Sym. on Combustion, The Combustion Institute, pp. 1355 ~1363.

Sichel, M. and Palaniswamy, s., 1984, "Sheath Combustion of Spray", Twentieth (Intl) Sym. on Combustion, The Combustion Institute, pp. 1789~1798.

Suzuki, T. and Chiu, H.H., 1971, "Multi-Droplet Combustion of Liquid Propellants", Proceedings of the Ninth International Symposium on Space Technology and Science, pp. 145 ~154.

Waldman, C.H., 1974, "Theory of Non-Steady State Droplet Combustion" Fifteenth(Intl) Sym. on Combustion, The Combustion Institute, pp. 429~441.

Williams, F.A., 1965, Combustion Theory, Addison Wesley Publishing Co., Inc., Reading, Mass··

APPENDIX

Calculaton of Boundary Conditions for a Vaporization Wave Structure

The boundary conditions on the differential equations, Eqs. (20, 21, 22) for the structure of the vaporization wave are obtained from the conservation of mass and energy across the wave.

(a) Overall Conservation of Mass Across the Wave

Flux of mass into wave

$$= U[4/3\ \pi\rho_l(n_1 a_{1i}^3 + n_2 a_{2i}^3) + (1 - 4/3\ \pi (n_1 a_{1i}^3 + n_2 a_{2i}^3))\rho_r] \tag{A1}$$

Flux of mass out of wave

$$= [\rho_v]\text{edge}$$
$$= -\rho_o{}^{w} v_o{}^{w} \cdot \rho_r \frac{\lambda}{\rho_r C_p R_i} + O(\varepsilon)$$
$$= -\phi_o{}^{w}(0) \cdot \rho_r \frac{\lambda}{\rho_r C_p R_i}$$
$$= -\frac{\lambda}{C_p R_i} \cdot \phi_o{}^{w}(0) \tag{A2}$$

Since the mass flux through the wave is constant, Eqs. (A_1, A_2) are equated to obtain

$$\phi_o^w(0) = -(c_p R_i/\lambda)\varepsilon U_o[4/3\pi\rho_1(n_1a_{1i}^3 + n_2a_{2i}^3) + (1-4/3\pi((n_1a_{1i}^3 + n_2a_{2i}^3))\rho_r]$$

where $U=\varepsilon U_o+\cdots\cdots$. And with the definitions for ε and γ_o and the approximation that $1-4/3\pi(n_1a_{1i}^3+n_2a_{2i}^3)\approx 1$, the boundary condition for the overall mass flux is obtained as

$$\phi_o^w(0) = \frac{1}{\gamma_o}\left[\frac{2}{3} + \frac{\rho_r/\rho_1}{(n_1a_{1i}^3 + n_2a_{2i}^3)}\right] \tag{A3}$$

(b) Conservation of Fuel Species Across the Wave

The flux of fuel species into wave is given by:

$$U = [4/3\pi\rho_1(n_1a_{1i}^3 + n_2a_{2i}^3) + (1-4/3\pi(n_1a_{1i}^3 + n_2a_{2i}^3))\rho_r\hat{Y}_r] \tag{A4}$$

There is no diffusive flux since there are no concertation gradients in the cloud interior. The flux of fuel species out of wave is given by:

$$\begin{aligned}\rho_v\hat{Y} - \rho D\frac{d\hat{Y}}{dr} &= \rho_v[\hat{Y}_r - \sqrt{\varepsilon}\,Y_o^w(0) - \frac{\rho D}{R_i\sqrt{\varepsilon}}\;\frac{\sqrt{\varepsilon}\,dY_o^w}{dr^w}\\ &= \frac{\lambda}{R_i c_p}[-\rho_o^w v_o^w \hat{Y}_r - \frac{dY_o^w}{dr^w}] + O(\sqrt{\varepsilon})\end{aligned} \tag{A5}$$

From the conservation of fuel species, it follws that Eqs. (A4, A5) can be equated to obtain:

$$\frac{dY_o^w}{dr^w}(0) = -\frac{2}{3\gamma_o}(1-\hat{Y}_r) \tag{A6}$$

(c) Conservation of Energy Across the Wave

From the conservation of energy it follows that: conductive heat flux into wave from ambient atmosphere

=heat absorbed by vaporizing droplets

+heat absorbed by vapor as it heats up from T_r to T_e, the edge temperature

Thus:

$$\lambda\frac{dT}{dr}(0) = \rho_r U c_p(T^e - T_r)\{1-4\pi/3(n_1a_{1i}^3 + n_2a_{2i}^3)\} + 4\pi/3(n_1a_{1i}^3 + n_2a_{2i}^3)\rho_1 U[L + c_p(T^e - T_r)] \tag{A7}$$

Since $\theta \equiv {}^c{}_p(T-T_r)/L$ and $U=\varepsilon U_o+\cdots\cdots$, Eq. (A7) may be written

$$\frac{d\theta^w}{dr^w}(0) = -\varepsilon^{3/2}\frac{\rho_1 U_o R_i c_p}{\lambda}\left[\frac{\rho_r}{\rho_1}\theta^w + \frac{4}{3}\pi(n_1a_{1i}^3 + n_2a_{2i}^3)(1+\theta^w)\right]_o$$

With the expansions Eq. (12), this becomes:

$$\frac{d\theta_o^w}{dr^w}(0) = -\varepsilon\frac{\rho_1 U_o R_i c_p}{\lambda}\frac{4}{3}\pi(n_1a_{1i}^3 + n_2a_{2i}^3)$$

With the definition of ε and γ_o it then follows that:

$$\frac{d\theta_o^w}{dr^w}(0) = -\frac{2}{3\gamma_o} \tag{A8}$$